Available online at www.sciencedirect.com
SCIENCE DIRECT®
Journal of Asian Earth Sciences 24 (2004) 259–270
Journal of Asian Earth Sciences
www.elsevier.com/locate/jaes

Orthomagmatic origin for the Ilkwang Cu–W breccia-pipe deposit, southeastern Kyongsang Basin, South Korea

Kyounghee Yang[a,*], Robert J. Bodnar[b]

[a]Geological Environmental Science Major, College of Science, Pusan National University, Pusan 609-735, South Korea
[b]Department of Geological Sciences, Virginia Polytechnic Institute and State University, Blacksburg, VA 24061, USA

Received 8 August 2003; accepted 2 December 2003

Abstract

Four distinct types of fluid inclusion are associated with brecciation, alteration and mineralization in the Ilkwang Cu–W breccia-pipe deposit in the southeastern Kyongsang Basin, South Korea. The earliest fluid inclusions in igneous quartz have salinities of 35–49 wt% NaCl equiv. and homogenize by halite dissolution. This fluid exsolved directly from the melt. A CO_2-bearing fluid (2–4 wt% NaCl equiv.) was trapped during the initial stages of brecciation and pressure decrease and later brecciation events and continued decreasing pressure in the magma chamber generated low-salinity, supercritical fluids that boiled to produce brine (40–48 wt% NaCl equiv.) and coexisting vapor (2–13 wt% NaCl equiv.) at 343–493 °C and 120–400 bars. The latest fluid (5–24 wt% NaCl equiv.) was trapped during the waning stages of hydrothermal activity. The oxygen and hydrogen isotopic compositions of the fluid ($\delta^{18}O_{SMOW} = 9.4–4.8‰$, $\delta D_{SMOW} = -45$ to $-49‰$) of quartz and the sulfur isotopic compositions ($\delta^{34}S_{CDT} = -0.3$ to $0.9‰$) of sulfide minerals cementing the breccia fragments, are consistent with a magmatic origin for the hydrothermal fluids. Fluid inclusion data and stable isotopic compositions suggest that Ilkwang Cu–W mineralization and alteration are products of orthomagmatic hydrothermal processes that were strongly pipe-controlled. The various types of fluid inclusions in the Ilkwang deposit reflect the evolution from a high pressure to a low pressure magmatic system. The evolution to a low pressure stage and concomitant aqueous fluid immiscibility in the Ilkwang deposit are major factors in the formation of economic mineralization.

Keywords: Fluid inclusions; Stable isotopes; Orthomagmatic; Fluid immiscibility

1. Introduction

A small granitic stock containing a Cu–W-bearing breccia-pipe deposit (referred to locally as the Ilkwang deposit) occurs in the southeastern Kyongsang Basin, South Korea (Fig. 1). Several studies have detailed the field relationships of the mineralization and the chemical and petrologic features of the host granite at the Ilkwang deposit (Fletcher, 1977; Jin, 1975; Kang et al., 1976). So and Shelton (1983) have examined the thermochemical nature and source(s) of the fluids responsible for alteration and mineralization at the Ilkwang deposit. They identified low to moderate salinity (0.5–12.0 wt% NaCl equiv.) fluids in the Ilkwang deposit, different from the high-salinity fluids typical of most other breccia-pipe deposits in silicic magmatic environments (Bodnar, 1995), but similar to those of other granite-associated tungsten deposits in Korea. These workers concluded that low to moderate salinity fluids may be typical of Korean W deposits, although they note that high-salinity (halite-bearing) inclusions had been found in the Dalsung breccia deposit. The absence of high-salinity fluids and lack of evidence for fluid immiscibility at Ilkwang has important implications in exploration, because previous workers (cf. Roedder and Bodnar, 1997) have emphasized the close association of high-salinity fluids, immiscibility, and economic mineralization in high-level silicic plutons. The present study was undertaken to better constrain the origin of the mineralizing fluids in the Ilkwang deposit, and to confirm the previously-reported absence of high-salinity fluids.

Fluid inclusions provide one of the best tools available to characterize the fluids responsible for mineralization

* Corresponding author. Tel.: +82-515-102247; fax: +82-515-176389.
E-mail address: yangkyhe@pusan.ac.kr (K. Yang).

1367-9120/$ - see front matter © 2004 Elsevier Ltd. All rights reserved.
doi:10.1016/j.jseaes.2003.12.001

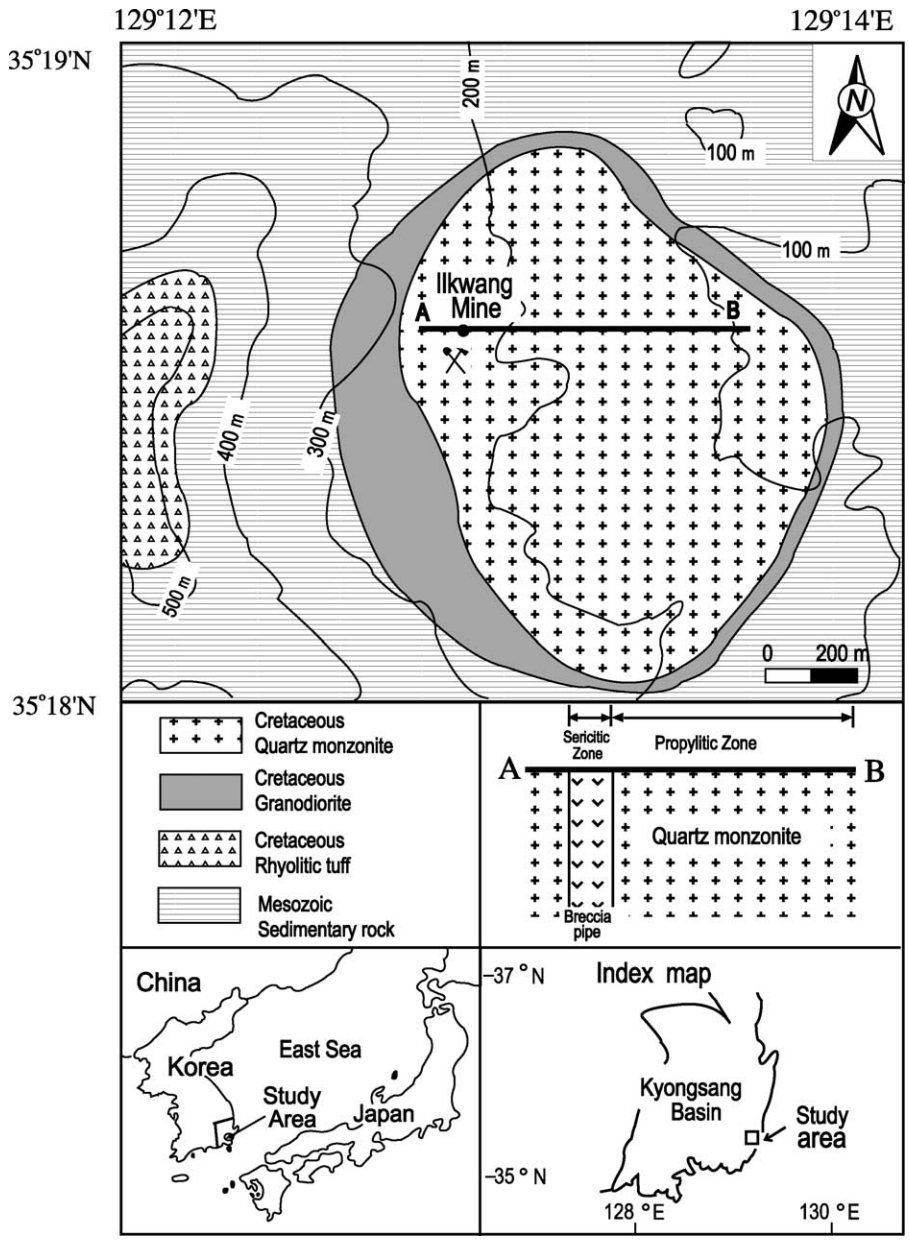

Fig. 1. Geologic map of the Ilkwang Cu–W mine area (after Fletcher, 1977).

and alteration in magmatic-hydrothermal systems (Bodnar, 1992, 1995). Recently, theoretical, experimental and laboratory studies of silicic magmatic systems have outlined a systematic and predictable pattern of fluid evolution during crystallization (Candela, 1997; Candela and Holland, 1984; Cline and Bodnar, 1991, 1994; Lynton et al., 1993). Specifically, the systematic variation in the partitioning behavior of chlorine between melt and coexisting magmatic fluid, as a function of pressure, allows the pressure evolution of the system to be inferred from microthermometric analysis of inclusions (cf. Cline and Bodnar, 1991). Thus, temperatures and salinities of fluid inclusions, combined with careful paragenetic studies, can be used to better understand fluid history during and following crystallization in a siliceous magmatic system.

The present study was undertaken to further constrain the evolution of the magmatic hydrothermal system at the Ilkwang deposit focusing on fluid inclusion microthermometric data and C, O, H and S stable isotopic data. The questions to be addressed in this paper concern the source and behavior of fluids involved in mineralization and alteration and the similarity of Ilkwang mineralization to granite-related mineralization elsewhere in the Circum-Pacific region. This paper presents a revised interpretation, documenting the important role of high-salinity magmatic

fluids and aqueous fluid immiscibility in the genesis of the Ilkwang Cu–W breccia-pipe deposit.

2. Geological setting

A small, elliptical stock hosting a mineralized breccia pipe intrudes a sequence of gently-dipping Upper Cretaceous basal shales and sandstones and overlying rhyolitic tuff in the southeastern Kyongsang Basin, South Korea (Fig. 1). The breccia pipe has surface dimensions of 100 by 70 m and dips nearly vertically. The margins of the pipe are defined by slickensided surfaces (Fletcher, 1977). The stock consists of a marginal phase and a central phase, which have been explained either as products of in situ differentiation of a single magma (Jin, 1975) or as separate intrusions (Fletcher, 1977). The stock is metaluminous to weakly paraluminous (Jin, 1975) and is hydrothermally altered, with the intensity of alteration increasing with proximity to the breccia pipe (Fig. 1). Sericitic alteration occurs near the pipe, grading outward to propylitic alteration (Fletcher, 1977; Jin, 1975). K–Ar dating of hornbende from the stock and sericite from breccia fragments within the pipe gave ages of 81 ± 3 and 69 ± 3 Ma, respectively (Fletcher, 1977).

The marginal phase of the stock at the contact with the sedimentary rocks consists of medium to fine-grained, grayish granodiorite containing plagioclase, K-feldspar, quartz, hornblende and biotite. The marginal phase contains more plagioclase and hornblende with equigranular to seriate texture, compared with the central phase of the stock. Some plagioclase and hornblende are altered to sericite, epidote and chlorite.

The central phase of the stock is a medium-grained, light gray quartz monzonite with seriate to porphyritic texture. The rock is composed of plagioclase, K-feldspar, quartz and biotite with minor hornblende. The intensity of propylitic alteration increases towards the pipe, and consists of epidote, chlorite, sericite, tourmaline and garnet, with alteration restricted mostly to feldspars and biotite. Plagioclase is typically dusted with sericite and most quartz is highly corroded. Biotite is the most abundant primary mafic mineral in the matrix, occurring as fine platy crystals with irregular grain boundaries. In many cases, biotite has been replaced by chlorite and sericite. Charcoal-like, black tourmaline occurs as rossettes, patchy clots, or isolated ragged crystals. The propylitically-altered rocks grade into sericite-altered rocks near the margin of the breccia pipe. The main difference between the two alteration zones is the presence of primary rock fabrics: primary textures are mostly obliterated in the sericitized rocks, whereas original textures are still recognizable in the propylitized rocks. Breccia blocks within the pipe are light brown and have been altered to epidote, chlorite, sericite, quartz, tourmaline and garnet. Sericite replaces feldspar and occurs as fine aggregates or large patches irregularly distributed in the matrix. Quartz occurs both as relict primary crystals and as secondary crystals in the matrix. Pink garnets, some of which are >0.5 cm in diameter, are disseminated throughout the granite near the pipe.

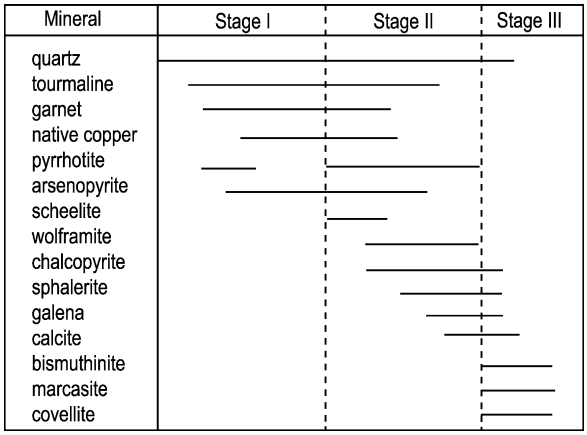

Fig. 2. Mineral paragenesis at the Ilkwang mine (after Kang et al., 1976).

The pipe contains angular to subangular granitic fragments showing clast-supported textures. The breccia blocks are cemented by quartz, tourmaline and massive chalcopyrite, arsenopyrite and pyrrhotite. The mineral paragenesis determined by previous workers (Fletcher, 1977; Kang et al., 1976) can be divided into three stages based on outcrop and microscopic observations (Fig. 2). Within the pipe, Stage I mineralization is represented by milky, granular or prismatic quartz, prismatic or acicular tourmaline, and disseminated garnet. Fine-grained milky, granular quartz precipitated on breccia fragments, sometimes shows comb structures. Native copper is sometimes observed on breccia fragments. Stage II mineralization is represented by milky to clear quartz, tourmaline and most ore minerals, suggesting that stage II represents the main stage of ore mineralization. Massive chalcopyrite, arsenopyrite and pyrrhotite are the dominant sulfides. Chalcopyrite occurs in veins with tourmaline, arsenopyrite and quartz. Scheelite occurs as light green fractured crystals surrounded by quartz. The last mineralization stage (Stage III) consists mainly of clear, euhedral quartz, chalcopyrite, sphalerite and galena. Calcite is the latest phase and occurs in the middle of veins, filling all remaining open space and typically associated with late, clear, euhedral quartz.

Replacement textures are common in the sulfides, and include alteration of chalcopyrite to covellite along fractures, chalcopyrite disease in sphalerite, replacement of pyrrhotite by marcasite, and atoll structures representing the selective replacement of arsenopyrite by chalcopyrite. Tear-shaped droplets of bismuthinite were observed within arsenopyrite.

3. Fluid inclusions

Fluid inclusions were examined to constrain the composition and temperature of fluids associated with

alteration and mineralization. Fluid inclusions were studied in igneous quartz from the host granitic rocks, in hydrothermal milky quartz, and in clear quartz and calcite from the matrix between breccia fragments representing different stages in the paragenetic sequence at Ilkwang.

Doubly-polished sections 0.07–0.1 mm thick were prepared for fluid inclusion petrography and microthermometric analyses. Four types of fluid inclusions were identified based on phase relationships at room temperature (Fig. 3). Type I inclusions are two-phase, liquid-rich, and low to moderate salinity (Fig. 3a and b). Type II inclusions are two phase, low salinity, and contain a vapor bubble that occupies greater than 80–90 vol.% of the inclusion at room temperature (Fig. 3c). Type III multiphase inclusions contain halite, vapor and several unidentified daughter minerals (Fig. 3(d) and (e)). Type III fluid inclusions are divided into two sub-types based on homogenization behavior: Type IIIa inclusions (Fig. 3d) homogenized by halite dissolution and Type IIIb inclusions (Fig. 3e) homogenized by vapor-bubble disappearance. These different modes of homogenization indicate different $P-T$ conditions of formation (Bodnar, 1994), as discussed in a later section. Type IIIa inclusions can often be identified at room temperature based on the large size of the halite crystal, compared to the vapor bubble, although identification must be confirmed by microthermometry. Type IV three-phase fluid inclusions contain liquid and gaseous CO_2, together with liquid H_2O, at room temperature (Fig. 3f).

3.1. Petrography

3.1.1. Igneous quartz

Igneous quartz from the host granitic rocks is cloudy and embayed and contains all four types of fluid inclusions. Most Type I, II and IV fluid inclusions in igneous quartz are secondary. Regular or negative crystal-shaped, primary Type IIIa inclusions (Fig. 3d) are relatively less abundant, small in size (< 10 μm), and randomly distributed. Type IIIa inclusions contain one or two birefringent daughter crystals, and, in most cases, opaque crystals, in addition to halite and vapor, indicating that the inclusions trapped a dense, complex hypersaline brine. Igneous quartz rarely contains Type IIIb fluid inclusions. Type IV regularly-shaped fluid inclusions (< 20 μm) cluster in groups or occur along microfractures, indicating a secondary origin.

3.1.2. Matrix milky quartz

Granular or prismatic quartz in the breccia matrix is typically cloudy and contains all types of fluid inclusions described above. Abundant secondary Type I, II, and IIIb fluid inclusions with various sizes cluster in groups or occur along microfractures. This hydrothermal quartz does not contain Type IIIa fluid inclusions. Negative crystal-shaped Type IV inclusions (Fig. 3f) are randomly distributed in three dimensional groups or clusters and contain both liquid CO_2 and H_2O with a narrow range of volume ratios

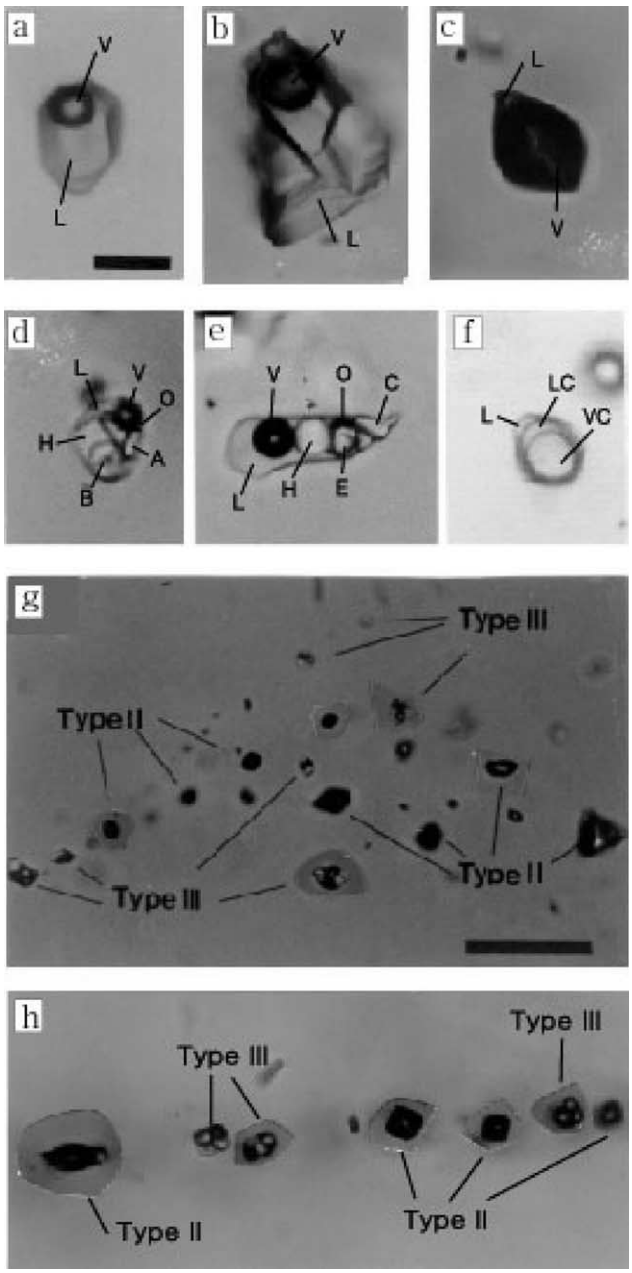

Fig. 3. Photomicrographs of different types of inclusions observed in quartz and calcite. All are from quartz except for 3b, which is from calcite. The scale bar in 3a represents 20 μm and applies to b–f. The scale bar in 3 g represents 80 μm and also applies to h. (a) Type I liquid-rich inclusions. (b) Type I liquid-rich inclusions in hydrothermal calcite. (c) Type II vapor-rich inclusions. (d) Type IIIa halite-bearing inclusions with four daughter minerals (halite, anhydrite, and two unidentified) in magmatic quartz. Note relatively large halite crystal and a small vapor bubble. (e) Type IIIb halite-bearing inclusions with four daughter minerals (halite, erythrosiderite with high refractive index, rhombic calcite, triangular opaque chalcopyrite (?)) in hydrothermal quartz. (f) Type IV liquid CO_2-bearing inclusions. A small amount of aqueous solution is visible along the wall. (g) Growth zones defined by numerous primary Types II and IIIb fluid inclusions in hydrothermal quartz. Note that vapor-rich inclusions (Type II) are generally larger than the saline inclusions (Type IIIb). (h) Primary or psudosecondary Type IIIb and II inclusions. L, liquid; V, vapor; H, halite; B, birefringent crystal; A, anhydrite; E, erythrosiderite; C, calcite; VC, liquid CO_2; LV, vapor CO_2.

(80–90%). Type IV inclusions are thought to post-date igneous quartz formation and to have been trapped during growth of milky quartz because Type IV inclusions were not observed in the late clear quartz, and occur only as secondary inclusions in igneous quartz.

Type II fluid inclusions coexisting with Type IIIb inclusions occur along growth zones (Fig. 3g) or along microfractures (Fig. 3h) that do not extend to the crystal boundary, indicating primary or pseudosecondary origin. These fluid inclusions were generally observed at the transition of milky to clear quartz and were trapped under boiling conditions. Thus, the homogenization temperature equals the formation temperature. Type IIIb fluid inclusions (Fig. 3e) contain halite, calcite, erythrosiderite(?) ($K_2FeCl_5 \cdot H_2O$?), chalcopyrite, one or two opaque grains, and a vapor bubble. Erythrosiderite is assumed from the transparent to pale green color, high refractive index, and strong birefringence (e.g. Stefanini and Williams-Jones, 1996). Some unidentified opaque daughter minerals may be hematite or chalcopyrite, based on the crystal shape and color (Bodnar, 1995; Mavrogenes and Bodnar, 1994). The relative size of the bubble in Type IIIb inclusions is larger than that in Type IIIa inclusions, implying different densities for these two fluids (Fig. 3d and e).

3.1.3. Clear quartz and calcite

Fluid inclusions in clear quartz and calcite from the breccia matrix contrast markedly with those in milky or igneous quartz. The fluid inclusions are rare and relatively large (up to 150 μm in diameter). Type I fluid inclusions are dominant. Clear quartz contains Type I and Type II fluid inclusions (Fig. 3a and c), whereas calcite contains only Type I primary fluid inclusions (Fig. 3b), representing the latest fluids trapped.

3.2. Microthermometry

Heating and cooling experiments were conducted using a Fluid Inc.-adapted USGS gas flow heating/cooling stage. The stage was calibrated at the triple points of CO_2 (−56.6 °C) and H_2O (0 °C) and at the critical point of H_2O (374.1 °C) using synthetic fluid inclusions. The accuracy and reproducibility of temperatures of phase changes are approximately ±0.1 °C at $T \leq 50\,^{\circ}C$ and ±0.5 °C at $T \leq 374.1\,^{\circ}C$. Salinities of aqueous inclusions were calculated using the program SALTY of Bodnar et al. (1989); salinities of CO_2-bearing inclusions were calculated from clathrate melting temperatures using the equation of Darling (1991). Phase changes observed during microthermometric analyses were liquid–vapor homogenization temperature (Th L–V); halite dissolution temperature (Tm halite); first melting or eutectic temperature (Te); clathrate melting temperature (Tm CO_2-clathrate); and the ice-melting temperature (Tm ice) (Table 1, Figs. 4 and 5). Groups of fluid inclusions that showed consistent homogenization temperatures were measured—inclusion groups that showed inconsistent homogenization temperatures were excluded from the study. These inconsistent temperatures could result from entrapment of two-phase mixture fluids containing vapor–liquid. The behavior of fluid inclusions during microthermometric analysis is discussed below, according to the location of the different inclusion types in the paragenesis, starting with the earliest Type IIIa inclusions.

3.2.1. Type IIIa fluid inclusions

Upon heating, vapor disappears between 217 and 385 °C. Halite dissolution occurs between 251 and 411 °C, and calculated salinities range from 35 to 49 wt% NaCl equiv (Bodnar et al., 1989). Halite dissolution is the final phase transition observed during heating experiments. Other transparent or birefringent daughter crystals do not dissolve during heating.

3.2.2. Type IV fluid inclusions

Homogenization temperatures of CO_2 to the vapor phase range from 26 to 28 °C, corresponding to CO_2 density of 0.30–0.25 g/cm^3 (Benard et al., 1985). Total homogenization to the vapor phase occurred between 301 and 330 °C. CO_2-clathrate melted at about 8–9 °C, corresponding to salinities of about 2–4 wt% NaCl equiv. (Darling, 1991). Combining Th CO_2, the clathrate melting temperature and the total homogenization temperature indicates a CO_2 concentration of 15–20 mol% in the system H_2O–CO_2–NaCl (Brown and Lamb, 1989; Hendee and Hollister, 1981). Solid CO_2 melted between −57.0 and −58.0 °C, indicating that the inclusion could contain as much as 10 mol% CH_4 (Hall and Bodnar, 1990).

3.2.3. Type IIIb and Type II fluid inclusions

Type IIIb fluid inclusions coexist with Type II inclusions and homogenize by vapor disappearance at 343–493 °C. Halite dissolution occurred between 323 and 405 °C, corresponding to salinities of 40–48 wt% NaCl equiv. (Table 1). Erythrosiderite (?) is the first phase to dissolve at 195–222 °C with a mode at 200–205 °C. During cooling following homogenization, erythrosiderite renucleated as aggregates of small grains rather than as a single crystal. Calcite, opaque daughter minerals, and other transparent daughter minerals did not dissolve, possibly because of hydrogen loss following entrapment (Mavrogenes and Bodnar, 1994). Vapor-rich fluid inclusions (Type II) remained unchanged during initial heating, followed by gradual vapor bubble expansion. This behavior made it difficult to measure the final bubble disappearance temperature and resulted in only estimates of Th (vapor), which ranged from about 432 to 519 °C (Table 1). As noted by Bodnar et al. (1985), vapor-rich inclusions trapped in a boiling system almost always trap some of the liquid along with the vapor, resulting in homogenization temperatures that are higher than the trapping temperatures. Thus, Bodnar and Vityk (1994) suggest that the homogenization

Table 1
Summary of fluid inclusion data from the Ilkwang Cu–W deposit

Host crystal	Type	Th (°C)	Tm (halite, °C)	Te (°C)	Tm (ice, °C)	Salinity (wt% NaCl)
Magmatic Quartz	IIIa	251–271(14)[a]	251–271			35–36
		284–293(9)	284–293			37–38
		312–323(11)	312–323			39–40
		338–346(7)	338–346			41–42
		353–374(10)	353–374			42–44
		380–391(9)	380–391			45–46
		403–411(6)	403–411			47–49
Hydro-Thermal Quartz	IV	301–316(45)		8.0–9.0:		4–2
		327–330(18)		Tm (CO_2-clathrate, °C)		
	IIIb	343–348(19)	333–339			41
		359–368(17)	330–350			41–42
		393–399(19)	372–375			44–45
		4s07–416(16)	309–383			40–45
		428–444(34)	310–362			40–43
		451–470(32)	365–405			44–48
		490–493(12)	323–324			41
	II	432–445(12)		−70.0	−1.0 to −9.2	1.7–13.1
		462–474(10)		–	−4.2 to −6.1	6.7–9.3
		485–492(5)		−75.4	−7.3 to −9.2	10.9–13.1
		513–519(2)			−7.2 to −7.7	10.7–11.3
	I	251–270(13)		−50.0 or below	−14.8 to −21.4	18.5–24.0
		281–284(9)			−18.1 to −20.7	21.0–22.2
		304–324(14)			−2.8 to −6.5	4.7–9.9
		331–337(8)			−5.1 to −7.0	8.0–10.5
Calcite	I	172–200(21)			−3.1 to −19.0	5.0–21.7
		206–225(33)			−3.8 to −19.3	6.2–21.9
		228–249(31)		−36.5	−7.9 to −15.6	11.6–19.2
		254–270(7)			−9.4 to −19.1	13.3–21.8

[a] () represents number of fluid inclusions measured.

temperatures of the liquid-rich inclusions in a boiling assemblage should be used to determine the temperature of homogenization and, therefore, the temperature of formation, of the boiling assemblage. We have followed this procedure here. Final melting of ice in the vapor-rich inclusions occurred between −9.2 and −1.0 °C, corresponding to salinities of 13.1–1.7 wt% NaCl equiv. The wide range in salinities is thought to be the result of trapping small amounts of liquid along with the vapor, as described above. Rarely, CO_2 was identified in Type II inclusions based on a melting event at approximately −56.6 °C, although a separate carbon dioxide fluid phase was never observed.

3.2.4. Type I fluid inclusions

Type I fluid inclusions trapped in clear and milky quartz have first melting temperatures below −50 °C, and final ice-melting temperatures between −2.8 and −21.4 °C (corresponding to salinities of 4.7–24.0 wt% NaCl equiv.). Type I inclusions homogenize between 251 and 337 °C. First-melting temperatures indicate the presence of cations other than sodium or potassium (Roedder, 1984)—the presence of calcite in this stage of the paragenesis suggests that the low first melting temperatures might be due to

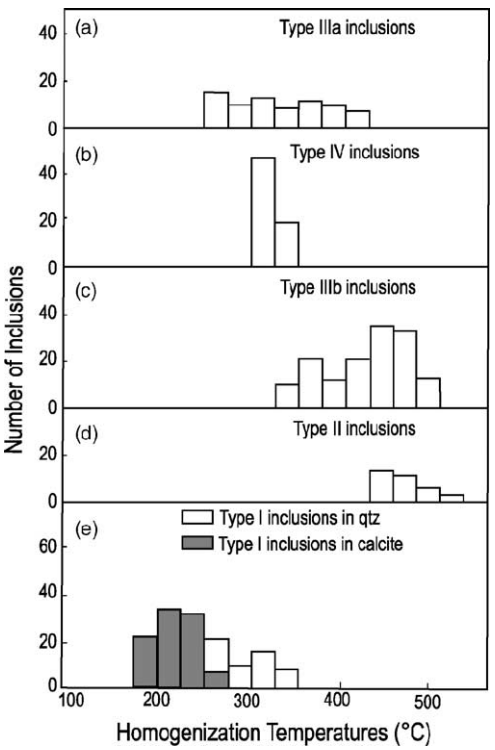

Fig. 4. Histogram of homogenization temperatures of fluid inclusions.

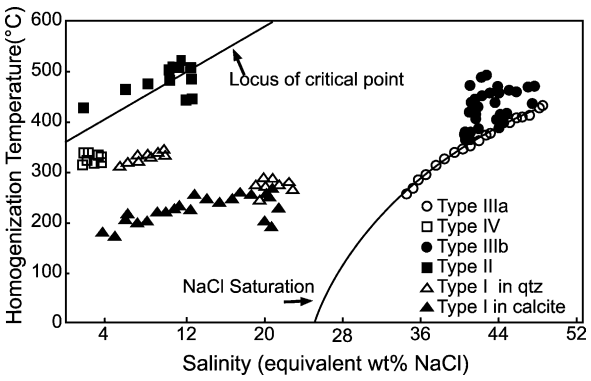

Fig. 5. Homogenization temperature—salinity relationships of fluid inclusions.

calcium in solution. Low to moderate salinity inclusions (4.7–10.5 wt% NaCl equiv.) show higher Th (304–337 °C) compared to higher salinity inclusions (18.5–24.0 wt% NaCl equiv.) with Th of 251–284 °C. Primary fluid inclusions in hydrothermal calcite show final ice-melting temperatures between −3.1 and −19.1 °C (corresponding to salinities of 5.0–21.8 wt% NaCl equiv.) and Th between 172 and 270 °C.

4. Stable isotopes

To help constrain the source of the mineralizing fluids, oxygen, sulfur and carbon isotopic compositions of quartz, sulfide minerals and calcite cements were measured (Table 2). Additionally, the hydrogen isotopic composition of water from fluid inclusions in quartz was measured. Results are reported in notation relative to SMOW for oxygen and hydrogen, CDT for sulfur, and PDB for carbon (Table 2). All stable isotope analyses were conducted at the Korea Basic Science Institute except for oxygen analysis of quartz, which was carried out at the University of Indiana, USA.

For δD analysis of fluid inclusions in quartz, quartz crystals were crushed and sieved to various grain size fractions in the range between 0.5 and 1 mm. The crushed materials were dried for at least 24 h at 120 °C under vacuum to eliminate adsorbed moisture on the quartz surfaces. Then, the materials were ground further and the released water was transferred to a Pyrex tube containing zinc metal. The glass tube containing water and zinc was heated to 500 °C for 30 min. Finally, the resulting H_2 gas was analyzed with a VG PRISM mass spectrometer. The precision of the δD measurements is better than ±1‰. For oxygen isotopic analysis of quartz, crystals were stored in vacuum at 120 °C for about 24 h before analyses. Oxygen was liberated using conventional BrF_5 methods of Clayton and Mayeda (1963). The extracted oxygen was converted to CO_2 gas and analyzed on a Finnnigan Delta-E ratio mass spectrometer. Analytical precision of $\delta^{18}O$ measurement is ± 0.05‰. The sulfur isotopic composition, $\delta^{34}S$, of arsenopyrite, chalcopyrite and pyrrhotite were measured. Analyses were performed by preparing sulfur dioxide through combustion with CuO at 1000 °C for 20 min. The error in analytical results is within ±0.2‰. For $\delta^{13}C$ and $\delta^{18}O$ analyses of calcite, samples were reacted with 100% H_3PO_4 at 90 °C, adopting the method of Swart et al. (1991). Carbon dioxide extracted during the reaction was analyzed using a VG PRISM mass spectrometer. Precision was maintained at better than ±0.2‰ for both $\delta^{13}C$ and $\delta^{18}O$.

Table 2
Hydrogen, oxygen, sulfur, and carbon isotope data in quartz, sulfide minerals, and calcite from the Cu–W Ilkwang deposit, Kyongsang basin, South Korea

Mineral	δD_{SMOW} (‰)	$\delta^{18}O_{SMOW}$ (‰)	$\delta^{18}O_{SMOW(water)}$ (‰) at 450 °C[a]	$\delta^{18}O_{SMOW(water)}$ (‰) at 350 °C	δ,$^{18}O_{SMOW(water)}$ (‰) at 250 °C	$\delta^{34}S_{CDT}$ (‰)	$\delta^{13}C_{PDB}$ (‰)
	−47	10.1	7.0	4.8			
MQuartz	−47	10.9	7.8	5.6			
	−45	12.5	9.4	7.2			
	−45	12.0	8.9	6.7			
	−49	11.8	8.7	6.5			
	−48	10.3	7.2	5.0			
Arsenopyrite						0.9	
						0.5	
Chalcopyrite						0.3	
						0.5	
Pyrrhotite						−0.3	
						−0.2	
Calcite					2.5		−5.0
					1.7		−5.0

[a] $\delta^{18}O$ of water from quartz has been calculated using the equilibration equation between quartz and water at 450 and 350 °C. $\delta^{18}O$ of water from calcite has been calculated at 250 °C.

The oxygen isotopic composition of hydrothermal quartz ranged from 10.1 to 12.5‰ (SMOW). The hydrogen isotopic composition of fluid inclusions in the same quartz ranged from −45 to −49‰ (SMOW). The $\delta^{18}O$ values of water that precipitated the quartz have been calculated assuming equilibration between quartz and water at 450 and 350 °C, as shown in Table 2 (Matsuhisa et al., 1979). These temperatures are based on the formation temperatures of primary fluid inclusions in the quartz. Using the measured range in the oxygen isotopic composition of the host quartz and the fluid inclusion temperatures, the calculated oxygen isotopic composition of the water ranges from 7.0 to 9.4‰ at 450 °C, and from 4.8 to 7.2‰ at 350 °C. These values suggest that the quartz precipitated from magmatic water (Fig. 6) and, because this quartz is closely associated temporally and spatially with alteration and mineralization in the breccia pipe (Fig. 2), suggests a magmatic origin for the mineralizing fluids.

There is little variation in $\delta^{34}S$ values of sulfides from the breccia pipe and the values are consistent with results from So and Shelton (1983). The narrow range of $\delta^{34}S$ values (−0.3 to 0.9‰) suggests a single magmatic source for the sulfur (Rye and Ohmoto, 1974). The sulfur isotopic composition of Ilkwang sulfides is similar to that measured in numerous porphyry copper deposits ($\delta^{34}S = -3$ to 1‰) (Rye and Ohmoto, 1974).

The $\delta^{13}C_{PDB}$ and $\delta^{18}O_{SMOW}$ of calcite are −5.0‰ and 9.0–9.8‰, respectively (Table 2). The $\delta^{18}O$ values of water that precipitated calcite were calculated assuming equilibration between calcite and water at 250 °C (Table 2), using the equation from Matsuhisa et al. (1979). Calculated $\delta^{18}O$ values of water associated with calcite deposition range from 1.7 to 2.5‰ and are not consistent with a magmatic origin (Fig. 6). However, the carbon isotopic composition of calcite is consistent with a mantle origin for the carbon (Rollinson, 1993).

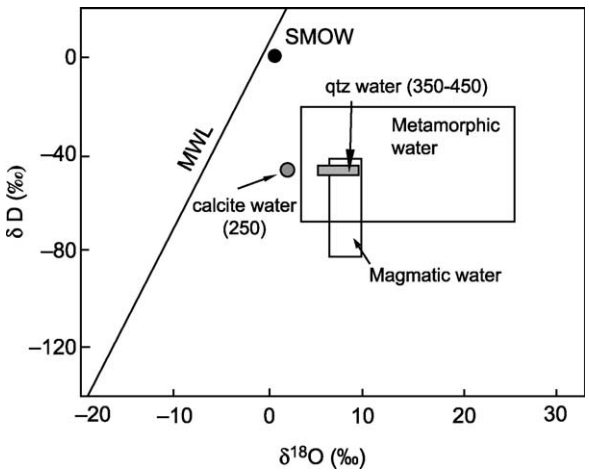

Fig. 6. Plot of measured δD vs calculated $\delta^{18}O$ for water in equilibrium with hydrothermal quartz at 350–450 °C (shaded box). The shaded circle represents the calculated oxygen isotopic composition of water in equilibrium with calcite at 250 °C. Also shown are the metamorphic and magmatic water boxes from Taylor (1979). MWL = Meteoric Water Line. SMOW = Standard Mean Ocean Water.

Stable isotopic data combined with geological and other geochemical data summarized above suggest that the early mineralising fluids at Ilkwang were predominately of magmatic origin. Results do not preclude a meteoric water contribution during the final stages of calcite precipitation (Fig. 6) as the intrusion cooled and the hydrothermal system collapsed, allowing externally-derived groundwaters to circulate through the deposit.

5. Discussion

5.1. Fluid inclusion geobarometry

Owing to the dynamic nature of the magmatic-hydrothermal system at Ilkwang, an overprinting of earlier inclusion generations by later inclusions makes it difficult to determine accurately the paragenesis or crosscutting relationships of fluid inclusions in individual samples. In spite of the inherent complications, the temporal evolution of the fluids may be inferred from detailed petrographic observations of fluid inclusions combined with the paragenetic sequence of their host crystals. The earliest inclusions are Type IIIa inclusions in magmatic quartz, followed by Type IV inclusions in hydrothermal milky quartz, followed by Type IIIb and II inclusions at the transition between milky and clear quartz. The latest fluids were trapped as Type I inclusions in clear quartz and calcite. The pressure–temperature evolution during trapping of the different generations of fluid inclusions described above is shown in Fig. 7, along with the H_2O-saturated solidus for a granodioritic melt containing 2 wt% B_2O_3.

Based on microthermometry and mineral equilibria, solidus temperatures of the Cretaceous–Tertiary granitic rocks in Kyongsang Basin fall in the range 580–670 °C at 1–2 kbars (Lee et al., 1995; Yang and Bodnar, 1994). Recent studies have demonstrated that the solidus temperature in a paraluminous, fluorine-enriched melt can extend to as low as 450–500 °C (Webster et al., 1987). In addition, the solidus temperature in a haplogranite system with 1.7 wt% B_2O_3 is depressed by more than 130 °C at 1 kbar, compared to the B-free system (Pichavant, 1981). The Ilkwang granitic rocks contains significant fluorine (285–103 ppm; Jin, 1975) and the presence of hydrothermal tourmaline confirms the presence of boron. The B_2O_3 concentration of a fluid in equilibrium with a paraluminous granitic melt crystallizing schorl-dravite was estimated at ~1.5 wt% (Benard et al., 1985). Thus, it is not improbable to assume that the solidus for the Ilkwang magma could have been depressed by perhaps 100 °C below that shown in Fig. 7. This would bring the solidus temperature for the Ilkwang magma into coincidence with the highest measured homogenization temperatures for fluid inclusions in the Ilkwang deposit (H500 °C).

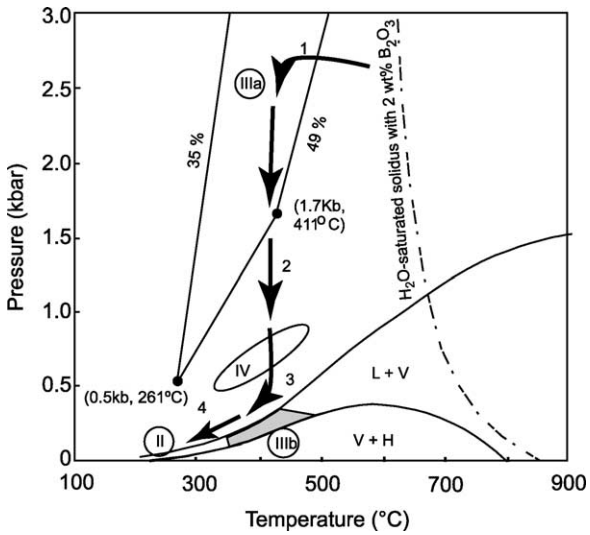

Fig. 7. Pressure-temperature evolution of the Ilkwang Cu–W breccia-pipe deposit in the Kyongsang Basin. The H_2O-saturated solidus for a granodiorite with 2 wt% B_2O_3 is interpolated from Pichavant (1981). Isochores for 35 wt% and 49 wt% NaCl were calculated using data from Bodnar and Vityk (1994). The arrow labeled 1, 2, 3 and 4 shows the P–T evolution path of fluids in the Ilkwang Cu–W breccia-pipe deposit inferred from fluid inclusions. The L + V area for NaCl-H_2O system is from Bodnar and Vityk (1994). The areas defined by IIIa, IV, IIIb, and II indicate the P–T trapping conditions for fluid inclusion types IIIa, IV, IIIb, and II, respectively. See the text for details.

The melting behavior indicates that Type IIIa inclusions, which represent the earliest fluid at Ilkwang, were trapped in the liquid-stable, vapor-absent field. Type IIIa inclusions that homogenize by halite disappearance also indicate higher densities of these inclusions compared to Type IIIb inclusions with the same salinity. The density differences indicate that Type IIIa inclusions were trapped at higher pressures than Type IIIb inclusions (Bodnar, 1994). In addition, the lack of cogenetic vapor-rich inclusions indicates that high-salinity fluids (Type IIIa inclusions) exsolved directly from the melt during the final stages of crystallization and were not a product of aqueous immiscibility (Bodnar, 1994; Cline and Bodnar, 1994). The trapping conditions for Type IIIa inclusions are thus constrained to lie within the P–T region defined by the isochores for 35 and 49 wt% NaCl shown in Fig. 7 (area 'IIIa'). Isochores for Type IIIa inclusions shown in Fig. 7 do not constrain the maximum pressure of trapping. Type IIIa inclusions could have been trapped at any pressure within the region bounded by the isochores, up to their intersection (not shown on Fig. 7) with the melt solidus. Note that if the solidus were depressed by about 100 °C from that shown on Fig. 7 (as a result of elevated B and/or F in the melt?), the isochores would intersect the solidus at about 550 ± 50 °C between about 2 and 3 kbars. This is also consistent with the maximum homogenization temperatures observed for the later Type IIIb inclusions.

The granitic magma is assumed to have crystallized from the walls of the magma chamber inward (cf. Burnham, 1979). The crystallizing magma produced an outer impermeable rind and the magma became overpressurised as water exsolved from the melt (Burnham, 1979). Type IIIa inclusions were trapped in this environment under essentially lithostatic pressure conditions. With continued crystallization and water exsolution (arrow '1' in Fig. 7), the pressure in the magma chamber eventually exceeded the tensile strength of the rock, leading to fracturing and brecciation of the overlying rocks. Breaching of the overlying confining rocks resulted in a pressure decrease and formation of the Ilkwang pipe (arrow '2' in Fig. 7). However, the pipe never breached the surface, based on field observations (Fletcher, 1977; Kang et al., 1976).

Pressure reduction accompanying breccia formation resulted in precipitation of milky quartz on breccia fragments and trapping of CO_2-bearing aqueous fluid inclusions (area IV in Fig. 7). The CO_2-bearing aqueous fluid (Type IV inclusions) was likely exsolved from the crystallizing magma during the pressure decrease. The narrow range of volume ratios and homogenization temperatures of randomly-distributed Type IV inclusions suggests that the inclusions were trapped in the one-phase field from a homogeneous CO_2–H_2O fluid. Compositions and microthermometric data indicate minimum trapping pressures of 450–600 bars. This pressure range was calculated assuming a Th of 300–330 °C, 3 wt% NaCl, and 20 mol% CO_2, based on the CO_2–H_2O–NaCl system (Bodnar et al., 1985; Brown and Lamb, 1989; Sterner and Bodnar, 1991). This pressure range is higher than that inferred by the later boiling pair as described below, supporting the interpretation that CO_2–H_2O–NaCl fluids were earlier than immiscible aqueous fluids described below. Hydrothermal alteration of the granite and precipitation of tourmaline started at this stage. In porphyry copper deposits, CO_2-rich fluid inclusions are generally associated with the early potassic and/or propylitic alteration, and usually predate or are concurrent with the early stage of copper mineralization (Beane and Bodnar, 1995). This observation is compatible with the results at Ilkwang.

Later brecciation events reduced the pressure in the system (arrow '3' in Fig. 7). The decreased pressure resulted in lower salinity fluids being exsolved from the melt (Cline and Bodnar, 1991). These low-salinity fluids boiled to generate brine (40–48 wt% NaCl equiv.) and coexisting vapor (2–13 wt% NaCl equiv.). This third hydrothermal stage is associated with deposition of massive sulfide minerals at temperatures between 343 and 493 °C, and at pressures between 120 and 400 bars (area IIIb). Pressures were calculated from vapor pressures for H_2O–NaCl (Bodnar and Vityk, 1994). The compositional ranges of coexisting Types II and IIIb fluid

inclusions are consistent with the experimental data of Benard et al. (1985).

The fourth and last hydrothermal stage was associated with low to moderate salinity fluids (Type I) that precipitated clear quartz and calcite. The late-magmatic, high-salinity fluids mixed with circulating meteoric fluids and were cooled and diluted to produce lower temperature, lower-salinity hydrothermal fluids that were trapped as inclusions during the final stage of hydrothermal activity (arrow '4' in Fig. 7).

5.2. Comparison of Ilkwang mineralisation to porphyry-type mineralisation in the Circum-Pacific region

Based on the geotectonic setting and the composition of granitic plutons in the Kyongsang Basin (Jin et al., 1981; Lee et al., 1987), it is logical to assume a genetic link between the base metal ore deposits and intrusive activity (Sillitoe, 1980; Min et al., 1982). Fluid inclusion data (Carson and Sawkins, 1980; Sillitoe and Sawkins, 1971; Yang and Bodnar, 1994) from Ilkwang is also consistent with results from porphyry-copper-associated, tourmaline-bearing breccia pipe mineralization elsewhere in the Circum-Pacific region. However, most granitic rocks in the Kyongsang Basin do not contain economic porphyry copper-type mineralization, although there is active exploration activity for copper deposits in this area (personal communication, Park and James, 2001). Yang and Bodnar (1994) suggested that the absence of economic mineralization in the Kyongsang basin is a result of the fact that the magmas were emplaced at greater depth and higher pressure (relative to typical porphyry copper magmas). As a result, the magmas either did not reach water saturation during crystallization, or did so late in the crystallization history after much of the copper had been lost to early-crystallizing ferromagnesian or oxide phases (Candela and Holland, 1984).

Abundant miarolitic cavities, primarily formed by lateral stretching of the roof rocks at relatively great depth (Burnham, 1979), are common in granitic rocks in the Kyongsang Basin (Koh, 2001; Yang and Bodnar, 1994). Most of the granites in the basin are massive and breccias are extremely rare. Unlike most other uneconomic granitic rocks in the Kyongsang Basin, the Ilkwang stock does not contain miarolitic cavities or pegmatites, but rather contains a breccia pipe indicating high pressures in the crystallizing magma, presumably associated with water exsolution from the magma. The stock appears to have either crystallized at a shallower depth, or perhaps the magma had a higher water content, compared with other granitic rocks in the basin. The level of emplacement of the Ilkwang granite appears to be similar to magmatic systems associated with porphyry copper deposits. This interpretation is supported by the occurrence of Type IIIb inclusions coexisting with Type II inclusions (Beane and Bodnar, 1995). Coexisting high salinity and vapor-rich inclusions, which are characteristic of shallow silicic plutons, are unknown or rare in other granites in the Kyongsang Basin.

Potassic alteration, common in porphyry copper deposits, is absent at the Ilkwang stock. Alteration in porphyry copper deposits is zoned from potassic alteration in the center of the pluton, to phyllic alteration near the pluton margins, with propylitic alteration in peripheral wall rocks (Beane, 1982). Phyllic alteration is often later and overprints an earlier lateral continuum of potassic alteration outward to propylitic alteration (Beane and Bodnar, 1995; Lowell and Guilbert, 1970). The Ilkwang stock is characterized by tourmalinised propylitic alteration at the margins, and grades into sericitic (phyllic) alteration in the breccia pipe. The absence of potassic alteration at Ilkwang suggests that the early fluids were potassium-depleted compared to early fluids in porphyry copper deposits. Sylvite (KCl), commonly found in fluid inclusions from porphyry copper deposits, is not observed in fluid inclusions in the Ilkwang stock, although the potassium-bearing phase erythrosiderite(?) ($K_2FeCl_5 \cdot H_2O$) is observed.

6. Conclusion

Fluid inclusion data and stable isotope results highlight the important role of magmatic waters in the formation of the mineralization at Ilkwang. The data indicate that brecciation, mineralization and alteration are products of hypogene orthomagmatic hydrothermal processes that were strongly pipe-controlled. No evidence was found to suggest that early fluid components were derived from wallrock by convective circulation of meteoric fluids and/or formation waters. The various types of fluid inclusions at the Ilkwang deposit reflect evolving fluid compositions and the effects of pressure fluctuations in the system. Unlike most other uneconomic granites in the Kyongsang Basin, the Ilkwang Cu–W deposit contains breccia pipes which indicate a relatively lower pressure or shallower depth of emplacement compared to other granites in the basin. The breccias are interpreted to have formed when water exsolved from the crystallizing magma, generating high pressures in the magma chamber. Fracturing of the overlying rocks produced the breccias and provided a conduit for magmatic fluids to exit the magma chamber.

Acknowledgements

We thank Dr Martin Feely for constructive criticism and advice for this paper. This work was partially supported by grant R04-2002-000-20045-0 from the Basic

Research Program of the Korea Science and Engineering Foundation.

References

Beane, R.E., 1982. Hydrothermal alteration in silicate rocks. In: Titley, S.R., (Ed.), Advances in Geology of the Porphyry Copper Deposits of Southwestern North America, University of Arizona Press, Tucson, pp. 117–137.

Beane, R.E., Bodnar, R.J., 1995. Hydrothermal fluids and hydrothermal alteration in porphyry copper deposits. In: Pierce, F.W., Bohm, J.G. (Eds.), Porphyry Copper Deposits of the American Cordillera, Arizona Geological Society Digest, pp. 83–93.

Benard, F., Moutou, P., Pichavant, M., 1985. Phase relations of tourmaline leucogranites and the significance of tourmaline in silicic magmas. Journal of Geology 93, 271–291.

Bodnar, R.J., 1992. Can we recognize magmatic fluid inclusions in fossil hydrothermal systems based on room temperature phase relations and microthermometric behavior? Geological Survey of Japan, Reports 279, 26–30.

Bodnar, R.J., 1994. Synthetic Fluid inclusions: XII. The system H_2O-NaCl. Experimental determination of the halite liquidus and isochores for a 40 wt% NaCl solution. Geochimica et Cosmochimica Acta 58, 1053–1063.

Bodnar, R.J., 1995. Fluid inclusion evidence for a magmatic source for metals in porphyry copper deposits. In: Thompson, J.F.H., (Ed.), Magmas, Fluids and Ore Deposits, Mineralogical Association of Canada Short Course 23, pp. 39–152.

Bodnar, R.J., Vityk, M.O., 1994. Interpretation of microthermometric data for H_2O–NaCl fluid inclusions. In: Vivo, B.D., Frezzotti, M.L. (Eds.), Fluid Inclusions in Minerals, Methods and Applications, Virginia Polytecnic Institute and State University, VA, pp. 117–130.

Bodnar, R.J., Burnham, C.W., Sterner, S.M., 1985. Synthetic fluid inclusions in natural quartz. III. Determination of phase equilibrium properties in the system H_2O–NaCl to 1000 °C and 1500 bars. Geochimica et Cosmochimica Acta 49, 1861–1861.

Bodnar, R.J., Sterner, S.M., Hall, D.L., 1989. Salty: A Fortran program to calculate compositions of fluid inclusions in the system NaCl–KCl–H_2O. Computers and Geoscience 15, 19–41.

Brown, P.E., Lamb, W.M., 1989. P–V–T properties of fluids on the system $H_2O \pm CO_2 \pm$ NaCl: new graphical presentations and implications for fluid inclusion studies. Geochimica et Cosmochimica Acta 53, 1209–1221.

Burnham, C.W., 1979. Magmas and hydrothermal fluids. In: Barnes, H.L., (Ed.), Geochemistry of Hydrothermal Ore Deposits, Second ed, Wiley, pp. 71–136.

Candela, P.A., 1997. A review of shallow, ore-related granites: texture, volatiles, and ore metals. Journal of Petrology 38, 1619–1633.

Candela, P.A., Holland, H.D., 1984. The partitioning of copper and molybdenum between silicate melts and aqueous fluids. Geochimica et Cosmochimica Acta 48, 373–380.

Carson, S.R., Sawkins, F.J., 1980. Mineralogic and fluid inclusion studies of the Turmalina Cu–Mo-bearing breccia pipe, Northern Peru. Economic Geolology 72, 1233–1237.

Clayton, R.N., Mayeda, T.K., 1963. The use of bromine pentafluoride in the extraction of oxygen from oxides and silicates for isotopic analysis. Geochimica et Cosmochimica Acta 27, 43–52.

Cline, J.S., Bodnar, R.J., 1991. Can economic porphyry copper mineralization be generated by a typical calc-alkaline melt? Journal of Geophysical Research 96, 8113–8126.

Cline, J.S., Bodnar, R.J., 1994. Direct evolution of brine from a crystallizing silicic melt at the Questa, New Mexico, Molybdenum deposit. Economic Geolology 89, 1780–1802.

Darling, R.S., 1991. An extended equation to calculate NaCl contents from final clathrate melting temperatures in H_2O–CO_2-NaCl fluid inclusions: implications for P–T isochore location. Geochimica et Cosmochimica Acta 55, 3869–3871.

Fletcher, C.J.N., 1977. The geology, mineralization, and alteration of Ilkwang mine, Republic of Korea. A Cu–W-bearing tourmaline breccia pipe. Economic Geology 72, 753–768.

Hall, D.L., Bodnar, R.J., 1990. Methane in fluid inclusions from granulites: A product of hydrogen diffusion? Geochimica et Cosmochimica Acta 54, 641–651.

Hendee, E.M., Hollister, L.S., 1981. An empirical solvus for CO_2–H_2O–2.6 wt% salt. Geochimica et Cosmochimica Acta 45, 225–228.

Jin, M.S., 1975. Geochemistry and copper mineralization of the granodiorite at Ilkwang Mine Gyeongsang-Namdo, Korea. MS Thesis, Seoul National University, Seoul, 61pp.

Jin, M.S., Kim, S.Y., Lee, J.S., 1981. Granitic magmatism and associated mineralization in the Gyeongsang Basin, Korea. Mining Geology 31, 245–260.

Kang, J.M., Chon, H.T., John, Y.W., 1976. Mineralization and origin of breccia pipe of Ilkwang tungsten–copper mine. Journal of Korean Institute of Mining Geology 13, 218–228 (in Korean with English abstract).

Koh, J.S., 2001. Mineralogical, geochemical and Sr–Nd isotopic characteristics of the Namsan A-type and Gyeongju I-type granitic rocks in the Kyongsang basin, Korea. PhD thesis, Pusan National University, 173pp.

Lee, M.J., Lee, J.K., Lee, M.S., 1995. Mineralogy and major element geochemistry of A-type alkali granite in the Kyeongju area, Korea. Journal of Geological Society of Korea 31, 583–607.

Lee, S.M., Kim, S.W., Jin, M.S., 1987. Igneous activities of the Cretaceous to the early Tertiary and their tectonic implications in South Korea. Journal of Geological Society of Korea 23, 338–359.

Lowell, J.D., Guilbert, J.M., 1970. Lateral and vertical alteration-mineralization zoning in porphyry ore deposits. Economic Geology 65, 373–408.

Lynton, S.A., Candela, P.A., Piccoli, P.M., 1993. Experimental study of the partitioning of copper between pyrrhotite and a high-silica rhyolitic melt. Economic Geology 88, 901–915.

Matsuhisa, Y., Goldsmith, J.R., Clayton, R.N., 1979. Oxygen isotope fractionation in the system quartz–albite–anorthite–water. Geochimica et Cosmochimica Acta 43, 1131–1140.

Mavrogenes, J.A., Bodnar, R.J., 1994. Experimental evidence and geologic implications of hydrogen movement into and out of fluid inclusions in quartz. Geochimica et Cosmochimica Acta 58, 141–148.

Min, K.D., Kim, O.J., Yun, S.K., Lee, D.S., Joo, S.W., 1982. Applicability of plate tectonics to the post-late Cretaceous igneous activities and mineralization in the southern part of South Korea (I). Journal of Korean Institute of Mining Geology, 123–154 (in Korean with English abstract).

Pichavant, M., 1981. An experimental study of the effect of boron on a water saturated haplogranite at 1 kbar vapor pressure. Contribution to Mineralogy and Petrology 76, 430–439.

Roedder, E., 1984. Fluid inclusions. Reviews in Mineralogy 12, 644.

Roedder, E., Bodnar, R.J., 1997. Fluid inclusion studies of hydrothermal ore deposits. In: Barnes, H.L., (Ed.), Geochemistry of Hydrothermal Ore Deposits, Third ed, Wiley, New York, pp. 657–698.

Rollinson, H., 1993. Using geochemical data: evaluation, presentation, interpretation. Longman Scientific and Technical, New York, 352 pp.

Rye, R., Ohmoto, H., 1974. Sulfur and carbon isotopes and ore genesis: a review. Economic Geology 69, 826–842.

Sillitoe, R.H., 1980. Evidence for porphyry-type mineralization in southern Korea. Mining Geology of Special Issue 8, 205–214.

Sillitoe, R.H., Sawkins, F.J., 1971. Geologic, mineralogic and fluid inclusion studies relating to the origin of copper-bearing tourmaline breccia pipes, Chile. Economic Geology 66, 1028–1041.

So, C.S., Shelton, K.L., 1983. A sulfur isotopic and fluid inclusion study of the Cu–W-bearing tourmaline breccia pipe, Ilkwang mine, Republic of Korea. Economic Geology 78, 326–332.

Stefanini, B., Williams-Jones, A.E., 1996. Hydrothermal evolution in the Calabona porphyry copper system (Sardinia, Italy): the path to an uneconomic deposit. Economic Geology 91, 774–791.

Sterner, S.M., Bodnar, R.J., 1991. Synthetic fluid inclusions. X: experimental determination of P–V–T–X properties in the CO_2–H_2O system to 6kb and 700°C. American Journal of Science 291, 1–54.

Swart, P.K., Burns, S.J., Leder, J.J., 1991. Fractionation of the stable isotopes of oxygen and carbon in carbon dioxide during the reaction of calcite with phosphoric acid as a function of temperature and technique. Chemical Geology 86, 89–96.

Webster, J.D., Holloway, J.R., Hervig, R.L., 1987. Phase equilibria of a Be, U, and F-enriched vitrophyre from Spor Mountain, Utah. Geochimica et Cosmochimica Acta 52, 2091–2107.

Yang, K., Bodnar, R.J., 1994. Magmatic-hydrothermal evolution in the bottoms of porphyry copper systems: evidence from the silicate melt and aqueous fluid inclusions in the Gyeongsang Basin, South Korea. International Geology Reviews 36, 608–628.